Direct Observation of Radical States and the Correlation with Performance Degradation in Organic Light-Emitting Diodes During Device Operation

Direct observation of radical states and the correlation with performance degradation in organic light-emitting diodes during device operation

Go Sato, Donghyun Son, Taisuke Ito, Fumiya Osawa, Yujin Cho, and Kazuhiro Marumoto*

Go Sato, Dr. Donghyun Son, Taisuke Ito, Fumiya Osawa, Prof. Kazuhiro Marumoto
Division of Materials Science, University of Tsukuba, Tsukuba, Ibaraki, 305-8573, Japan
E-mail: marumoto@ims.tsukuba.ac.jp
Dr. Yujin Cho
Nano Device Characterization Group, Nano-Electronics Materials Unit, WPI Center for
Materials Nanoarchitectonics (MANA), National Institute for Materials Science (NIMS), 1-1
Namiki, Tsukuba, Ibaraki 305-0044, Japan
Prof. Kazuhiro Marumoto
Tsukuba Research Center for Interdisciplinary Materials Science (TIMS), University of
Tsukuba, Tsukuba, Ibaraki, 305-8571, Japan

Abstract

Microscopic characterization of radical states in organic light-emitting diodes (OLEDs) during device operation is useful for elucidating the degradation mechanism because the radical formation has been considered as non-radiative recombination centers. Electron spin resonance (ESR) spectroscopy is suitable for such characterization because it can directly observe radicals in OLEDs. In this work, the detailed ESR investigation into the radical states in OLEDs during device operation is firstly reported using a typical light-emitting Alq_3-based OLEDs. The simultaneous measurements of the ESR signal and the luminance of the same OLED are performed to study the direct correlation between the radical states and the performance degradation. These characteristics show that the luminance monotonically decreases and an ESR signal concomitantly increases as the duration of the device operation increases after operating the OLED. Using the analysis of density functional theory (DFT) calculation, the origin of the newly emerged ESR signal is ascribed to the cationic species due to decomposed Alq_3 molecules. The elucidation of the radical species formed in OLEDs during device operation has been demonstrated at a molecular level for the first time. This ESR analysis would provide useful knowledge for understanding the degradation mechanism in the OLEDs at the molecular level.

1. Introduction

Organic light-emitting diodes (OLEDs) have been attracting much attention as a next-generation display and illumination instead of liquid-crystal displays because they show high efficient luminescence and have advantages such as light weight and flexible.[1-6] The practical layered-type OLED based on tris(8-hydroxyquinoline) aluminum (Alq_3) used as a luminescent layer has been reported in 1987.[7] Thereafter, the OLEDs based on the luminescent material Alq_3 and a hole transport material N,N'-diphenyl-N,N'-bis(1-naphthyl)-1,1'-biphenyl-4,4'-diamine (NPB) have been studied as a typical device.[8-19] For the performance improvement and the understanding of the degradation mechanism of the OLEDs, the elucidation of charge and defect states in OLEDs is indispensable. In the study of the degradation mechanism of the OLEDs based on Alq_3 and NPB, it has been discussed that the generated cationic Alq_3 species during device operation act as fluorescent quenchers and cause the device degradations.[9] Also, in the study of thermally stimulated current measurements, the trappings of hole and electron carriers in Alq_3 have been reported.[10] Recently, for the degradation mechanism of the OLEDs based on Alq_3 and NPB, it has been discussed that the two degradation processes take place during device operation with a constant current.[11] For the first stage of the degradation, which is abbreviated as the fast degradation hereafter, the decomposition of NPB molecules has been suggested, which is considered to form trapping levels and quenchers in the OLEDs.[12-14] For the second stage of the degradation, which is abbreviated as the slow degradation hereafter, the generation of the cationic Alq_3 species by the reactions with moisture and oxygen[15,16] and the generation of the quenchers by ultraviolet (UV) light irradiation[17-19] have been suggested. However, the degradation mechanisms of the OLEDs including the devices based on Alq_3 and NPB have not yet been completely understood at a molecular level.

For investigating organic devices such as the OLEDs and the constitution materials at a molecular level, electron spin resonance (ESR) spectroscopy is one of most suitable techniques because the ESR method is a highly sensitive and nondestructive technique for directly observing radicals and charges with spins in organic semiconductors and their devices at a molecular level.[20-26] The ESR studies have demonstrated a clear correlation between the performance deterioration and the charge (and spin) accumulation (or deep trappings) in photovoltaic devices, and have clarified the degradation mechanism due to the charge (and spin) formation during device fabrication.[22,25] In the ESR study of the OLED based on 4,7-diphenyl-1,10-phenanthroline (BPhen), the correlation between the radical formation and the luminance degradation during devices operation has been discussed.[21] However, the radical species has not yet been identified at a molecular level.[21] Moreover, the ESR study for the radical species in other OLEDs during device operation has not yet been performed at a molecular level.

Here, we report the first detailed investigation into the radical states in OLEDs using the ESR spectroscopy. We simultaneously measured the dependence of the ESR signal and the luminance of the same OLED based on Alq_3 and NPB on the duration of the device operation, with no uncertainty in the reproducibility due to device quality, which showed a correlation between the ESR signal and the performance degradation. From the analysis using density functional theory (DFT) calculations, we identified that the origin of the newly emerged ESR signal is ascribed to the cationic species of decomposed Alq_3 molecules for all stages of the degradation, not to cationic species of NPB or decomposed (or degraded) NPB molecules previously discussed. Thus, we strongly suggest that the origin of the fast degradation of the device is ascribed to the formation of the cationic decomposed Alq_3 molecules at the molecular level. Also, we ascribe the origin of the slow degradation to the formation of the cationic decomposed Alq_3 species at the molecular level, which is consistent

with that of the previous works using macroscopic experimental methods and theoretical calculations.[15-19]

2. Result and discussion

2.1. Fabrication and Characterization of OLEDs

To attain a high signal-to-noise (SN) ratio of the ESR signal by increasing the active area of the device, we utilized a rectangular device structure (3 mm×20 mm) in an ESR sample tube with an inner diameter of 3.5 mm and with a length of 270 mm.[22,27] **Figure 1** shows the device structure of indium-tin-oxide (ITO) (150 nm)/NPB (60 nm)/Alq$_3$ (60 nm)/LiF (0.5 nm)/Al (100 nm) used in this study. It has been reported that the use of LiF/Al for the cathode largely improves the efficiency of electron injection into Alq$_3$ compared with metal electrodes.[28,29] The ITO substrate (3 mm×20 mm) was cleaned by the ultrasonic treatment with organic solvents, and by the treatments of oxygen plasma and UV ozone. The layers of NPB, Alq$_3$, LiF, and Al were vapor-deposited sequentially using a thermal evaporation method under 8×10^{-5} Pa. The active area was 0.2 cm^2. The layer of Alq$_3$ has been reported to act as the emitting layer in the device, in other words, the recombination zone of charge carriers, and the layer of NPB has been reported to act as the hole transport layer in the device.[8] The fabricated device was fixed on a device holder, a polyethyleneterephthalate (PET) film with a size of 3 mm × 250 mm, because the device holder is needed to transfer the device into the ESR sample tube. The quartz substrate and the PET device holder are non-magnetic. After wiring, the device was sealed in the ESR sample tube in an N$_2$-filled glove box (O$_2 \leq$ 0.5ppm, H$_2$O $\leq$ 0.5 ppm). We attempted to prevent the large degradation due to moisture using a desiccant to obtain the standard operation of the device. Although we performed careful treatment for reducing oxygen and moisture in the ESR sample tube, slight oxygen and moisture seem to be remained in the inside of the ESR sample tube because the atmosphere in the glove box contains O$_2 \leq$ 0.5ppm and H$_2$O $\leq$ 0.5

ppm and the PET film is known to contain moisture inside, which resulted in the observation

of very weak ESR signals, as described below.

The fabricated OLEDs were simultaneously measured using a JEOL RESONANCE

JES-FA200 X-Band ESR spectrometer and a TOPCON BM-9M luminance meter. A standard

Mn^{2+} marker sample was used to calibrate the g factor, the ESR linewidth, and the number of

spins (N_{spin}). The N_{spin} was evaluated by integrating the ESR spectrum twice and by

comparing the standard Mn^{2+} marker sample. The OLEDs was driven using a Keithley

2612A source meter at a constant current density $J = 40$ mA cm^{-2}. All measurements were

conducted at room temperature.

2.2. Luminance Degradation Characteristics

First, we describe the luminance degradation characteristics of the fabricated OLEDs

during device operation. The blue open circles in **Figure 2** show the dependence of the

luminance of the OLED on the duration of the device operation. The initial luminance of the

OLED was 760 cd m^{-2} at a constant current density of 40 mA cm^{-2}. After 1 h device

operation, the luminance decreased to approximately 80% of the initial luminance, and

thereafter it slowly decreased to approximately 45% of the initial luminance after 60 h device

operation. We have performed the fitting analysis to evaluate the decay process of the

luminance using the following exponential functions:

$$L = A_1 \exp\left(-\frac{t}{\tau_1}\right) + A_2 \exp\left(-\frac{t}{\tau_2}\right) + A_3 \exp\left(-\frac{t}{\tau_3}\right). \tag{1}$$

Here, A_1, A_2, and A_3 represent the relative intensity of the luminance and τ_1, τ_2, and τ_3

represent the decay time constant of the luminance for each exponential function, respectively.

Using the fitting analysis, the experimental result can be described by the sum of three

exponential functions as shown by the red solid line in Figure 2. The obtained fitting

parameters of each constant is $\tau_1 = 0.2$ h (orange dotted line, $A_1 = 16\%$), $\tau_2 = 6$ h (purple

dotted line, $A_2 = 14\%$), and $\tau_3 = 140$ h (green dotted line, $A_3 = 70\%$). From this fitting

analysis, we have found that the luminance degradation has three stages of initial, fast, and

slow degradation. The fast and slow degradation may correspond to those of the previous

studies.[11,30] For the initial degradation, by very carefully looking at the date of the previous

literature, one can find a sudden decrease in the luminance just after device operation.[11] This

origin has not yet been discussed previously,[11] which may correspond to the initial

degradation of the present study. We have simultaneously performed the ESR measurements

of the same OLED to elucidate the degradation mechanism in the device, which shows the

correlation between the luminance degradation and the change in the radical states in the

OLED, as described below.

2.3. ESR Signals of the OLED before and after Device Operation

Direct evidence for the radical formation in devices is demonstrated by the ESR

measurements. In these experiments, a continuous-wave method with a modulation frequency

of 100 kHz for the external magnetic field H was used.[25] Thus, spin-accompanied charge

carriers with a lifetime of <10 μs, which contributed to the normal operation of the device,

cannot be observed in this ESR method. Hence, the observed ESR signals are due to stably

formed radicals or accumulated (or deeply trapped) charge (and spin) carriers with a lifetime

of >10 μs. The upper data of **Figure 3** shows the ESR spectrum before the device operation

as a function of H. We have performed the fitting analysis for this spectrum. **Figure 4**a

shows the fitting results. The ESR spectrum before the device operation is described by a

Lorentzian function as shown by the green solid line, which is defined as Signal A hereafter.

For the ESR parameters, the g factor and the peak-to-peak ESR linewidth ΔH_{pp} were

determined as $g = 2.0030 \pm 0.0003$ and $\Delta H_{pp} = 0.85 \pm 0.02$ mT, respectively. Here, the g factor

was evaluated from the resonance magnetic field where the ESR spectrum with a first

derivative form has a value of zero, and the ΔH_{pp} value was evaluated as the difference

between the two magnetic fields at a peak and a valley in the ESR spectrum. The g factor obtained by the fitting analysis is consistent with that of the Alq_3 radial anions ($g = 2.0028$) obtained from the previous ESR study for Li-doped Alq_3 films[26] and that obtained from the DFT calculation.[23] From this consistency, the origin of the Signal A is ascribed to the Alq_3 radical anions formed by electron doping due to the reaction at the interfaces of Alq_3/LiF/Al layer: $3LiF + Al + 3Alq_3 \rightarrow AlF_3 + 3Li^+Alq_3^-$.[31,32]

To study the radical formation in the OLED after device operation, we simultaneously measured the ESR signal and the luminance of the same OLED during device operation. A middle data of Figure 3 shows the ESR spectrum of the OLED after 1 h device operation as a function of the H. From the comparison with the upper data of Figure 3, the ESR signal was confirmed to clearly increase after 1 h device operation. **Figure 4**b shows the result of the fitting analysis of the ESR spectrum. The ESR spectrum cannot be described by the only Signal A observed before the device operation. The ESR spectrum can be explained by the sum of two components (orange solid line) of a Lorentzian function (green dotted line) and a Gaussian function (red dotted line). The ESR parameters of the Lorentzian component (green dotted line) were determined as $g = 2.0030 \pm 0.0003$ and $\Delta H_{pp} = 0.72 \pm 0.02$ mT, respectively. Since this g factor is consistent with that of the Signal A obtained before the device operation, we identify the origin of the Lorentzian component as the Alq_3 radical anions, and assign the signal as the Signal A. However, the ESR parameters of the Gaussian function (red dotted line) were determined as $g = 2.0043 \pm 0.0003$ and $\Delta H_{pp} = 1.60 \pm 0.02$ mT, respectively, which are clearly different from those of the Signal A. Hereafter, we define the Gaussian component as the Signal B. We have also experimentally confirmed this newly emerged ESR signal after the device operation by directly subtracting the ESR signal before the device operation from that after the device operation. It is found that the newly emerged ESR spectrum obtained by subtracting ESR spectrum before the device operation (the upper data of Figure 3) from that

after 1h device operation (the middle data of Figure 3) has the g factor of $g = 2.0043$, that is, that of the Signal B. The lower data of Figure 3 shows an ESR spectrum after 60 h device operation. Since this ESR spectrum is described by the sum of components of the Signal A and the Signal B, no additional signal component was confirmed, where the only intensity of the ESR signal decreased in comparison with that of the ESR signal after 1 h device operation. This decrease is ascribed to the decrease in the intensity of the Signal A, and the intensity of the Signal B, whose origin is due to the degradation, increases with increasing the duration of device operation, as discussed later.

2.4. Correlation between the Radical States and the Luminance During Device Operation

It is interesting to investigate the correlation between the radical states and the luminance of the same OLED during device operation. **Figure 5** shows the dependence of the number of spins (N_{spin}) obtained from the ESR signal and the luminance of the OLED on the duration of the device operation at $J = 40$ mA cm^{-2}. As the luminance decreased, the N_{spin} of the Signal A slowly decreased with the device operation. Therefore, this result indicates that the number of Alq$_3$ radical anions in the OLED decreases as the duration of the device operation increases; the reason will be discussed in 2.6. However, the N_{spin} of the Signal B suddenly increased after 1 h device operation, and thereafter slowly increased as the duration of the device operation increased. As a result, the sum of the N_{spin} of the Signal A and the Signal B (Total N_{spin}) suddenly increased after 1 h device operation, and then slowly decreased. Since it has been reported that the formation of Alq$_3$ anions does not contributed to the luminance degradation,[9] the Signal B would contribute to the luminance degradation, especially to the initial degradation. In the previous studies, the origins of the fast and the slow degradation have been ascribed to decomposed (or degraded) NPB molecules and

decomposed Alq₃ molecules, respectively.[11-19] Thus, in the following subsection, we discuss the origin of the Signal B.

2.5. Origin of the Radical Formation Related with the Luminance Degradation

In this subsection, the origin of the Signal B is discussed for the luminance degradation. The previous studies has discussed that the fast degradation is due to the radical formation of decomposed (or degraded) NPB molecules and that the slow degradation is due to the quenchers of decomposed Alq₃ molecules.[11-19] Thus, there is two possibilities for the origin of the Signal B. The first possibility is the radical formation due to NPB or decomposed (or degraded) NPB molecules during device operation.[12-14] The second possibility is the radical formation due to Alq₃ or decomposed Alq₃ molecules during device operation.[15-19]

First, we discuss the first possibility of the radical formation in NPB or decomposed (or degraded) NPB molecules as the origin of the Signal B. It has been discussed that the decomposed (or degraded) NPB molecules due to the device operation of OLEDs create hole trappings sites and the trapped holes in the sites cause the luminance degradation.[12-14] Also, the neutral radical formation due to decomposed (or degraded) NPB molecules has been discussed to cause the luminance degradation.[12-14] Thus, to identify whether these proposed molecules are the origin of the Signal B or not at the molecular level, we have studied the radical states of these molecules using DFT calculations. We utilized the B3LYP functional and the 6-31G(d,p) basis set for the DFT calculations. **Figure 6** shows the chemical structures of the NPB and the decomposed NPB molecules which have been tentatively proposed in the literatures.[13,14] We define the proposed decomposed NPB products as PN1-PN6 in this work. The calculated spin density distributions for the cationic radical states of NPB and PN1-PN5 and for the neutral radical state of PN6 are shown in Figure 6. **Table 1**

shows the calculated principal values of the g tensor (g_1, g_2, g_3) and the average values of the three principal values (g_{ave}). **Figure 7** shows the chemical structures of the degraded NPB molecules which have been tentatively proposed in the literature.[14] We define the proposed degraded NPB products as DN1-DN6 in the present study. The calculated spin density distributions for the neutral radical states of DN1-DN6 are shown in Figure 7. **Table 2** shows the calculated principal values of the g tensor (g_1, g_2, g_3) and the g_{ave}. From Table 1 and 2, all the g_{ave} of the cationic and the neutral radical states of the NPB or the decomposed (or degraded) NPB molecules are not consistent with the g factor of the Signal B ($g = 2.0043$). Therefore, the radical formation from the NPB or the decomposed (or degraded) NPB molecules is excluded from the origin of the Signal B which correlates with the luminance degradation. In the cases of the NPB-related materials, the calculated g factor is almost similar with each other in cationic radical states (Table 1) or neutral radical states (Table 2), and the similar spin density distribution has been obtained in cationic radical states (Figure 6) or neutral radical states (Figure 7), respectively. This consistency reasonably explains the correlation between the calculated g factor and the spin density distribution.

To further exclude the possibility of the radical formation due to NPB-related molecules from the origin of the Signal B, we have examined the contribution of halogens remained in NPB molecules. It has been reported that the g factor of NPB molecules becomes larger by iodine doping to NPB molecules.[33] In addition, halogens are generally used for the NPB synthesis and may possibly be remained in NPB molecules. Actually, it has been reported that the g factor of the ESR signal of a conducting polymer poly(3-hexylthiophene) (P3HT) becomes larger by bromines remained at polymer-chain ends of P3HT.[27,34] To examine the possibility of remained halogens, we performed the quantitative analysis of the content of halogens in the NPB material used in this study. The ion chromatography analysis of the NPB sample showed that iodine and bromine were not detected and chlorine was

confirmed to be very small and less than 5 μg for the NPB sample of 0.056 g. Moreover, the fluorescent X-ray spectroscopy of the NPB sample showed no peak due to iodine, bromine, and chlorine. Therefore, the possibility of remained halogens in NPB molecules is experimentally excluded, which further excludes the possibility of the radical formation due to the NPB-related molecules from the origin of the Signal B.

Next, we discuss the second possibility of the radical formation due to the Alq_3 or the decomposed Alq_3 molecules as the origin of the Signal B. It has been discussed using current-voltage and photoluminescence (PL) methods that the accumulation of cationic Alq_3 in OLEDs contributes to the device degradation.[9] In the recent study, the degradation mechanism due to the decomposed Alq_3 under UV light irradiation has been discussed using PL and infrared (IR) spectroscopy methods.[11,17-19] To investigate the possibility of the radical formation due to the Alq_3 or the decomposed Alq_3 molecules at the molecular level, we performed the DFT calculation for radical cationic states of these molecules to compare with the ESR results. We used the B3LYP functional and the 6-31G(d,p) basis set for the DFT calculation. **Figure 8** shows the chemical structures of Alq_3 and decomposed Alq_3 molecules which have been tentatively proposed in the literatures.[19] We define the proposed decomposed Alq_3 products as PA1-PA5 in this work. The calculated spin density distributions of the radical cationic states are shown in Figure 8. **Table 3** shows the calculated principal values of the g tensor (g_1, g_2, g_3) and the g_{ave}. From Table 3, the cationic species of Alq_3 and PA2-PA5 show $g_{ave} = 2.0040$-2.0041. These g factors well correspond to that of the Signal B of $g = 2.0043 \pm 0.0003$. However, the g_{ave} of the cationic PA1 ($g_{ave} = 2.0029$) does not correspond to the g factor of the Signal B. This disagreement is consistent with the previous work where the PA1 is unlikely the origin of the photo degradation of Alq_3 from the IR study.[19] The calculated g factor of PA1 ($g_{ave} = 2.0029$) is significantly different from those of other Alq_3-related materials ($g_{ave} = 2.0040$-41). This difference is attributed to

12

the difference in spin density distribution shown in Figure 8, where PA1 has a different spin density distribution compared with those of other Alq_3-related materials. In addition, the PL study of hole-only devices has discussed that the cationic species of Alq_3 has little contribution to the luminance degradation.[11] Thus, the cationic species of the PA2-PA5 are possibly the origin of the Signal B that relates with the initial, fast, and slow degradation. Further study for a different set of Alq_3 structures is an interesting issue. However, the formation of anionic Alq_3 has been reported to have no relation with the luminance decrease.[9] Also, except for Ref. 19, the study for degraded components of Alq_3 has not yet been reported. The study of other decomposed cationic Alq_3 seems to have no basis for justifying the execution of the research because there are no report for other decomposed cationic Alq_3. Further ESR study combined with other spectroscopic methods such as PL and IR is an interesting topic, which is currently in progress and will be reported in a separate paper.

Our study have discussed the three stages of initial, fast, and slow degradation for the luminance of the OLEDs. Also, we have proposed that the formation of the cationic decomposed Alq_3 molecules contributes to the luminance degradation. Although the fast degradation due to the decomposed (or degraded) NPB molecules have been discussed,[11-19] the fast degradation of the present OLEDs is likely due to the formation of the cationic decomposed Alq_3 molecules, as discussed above. The PL and IR studies have discussed that the fast and slow degradations occur at the NPB/Alq_3 interface and in bulk Alq_3 molecules, respectively.[11-19] Thus, we suggest that three degradation stages are ascribed to the formation of the cationic decomposed Alq_3 molecules where the initial degradation occurs at the NPB/Alq_3 interface, the fast degradation occurs in the vicinity of the NPB/Alq_3 interface, and the slow degradation occurs in bulk Alq_3 molecules.

Further experiment using hole-only devices (HODs) is useful for further confirming the origin of the Signal B as the decomposed Alq_3 molecules and for eliminating the possibility of the interaction between NPB and Alq_3 during the device degradation. We performed the ESR study for the HOD with the device structure of ITO/Alq_3 (60 nm)/Au (50nm), which was fabricated using a thermal evaporation method under 8×10^{-5} Pa. The active area was 0.2 cm^2. To examine the Alq_3 degradation in the HOD, we measured the ESR signal of the HOD in the ESR sample tube with the application of the same current density used for the OLED under ultraviolet (UV) exposure. The experiment atmosphere of the HOD was the same as that used for the OLED, that is, under an N_2-filled glove box ($O_2 \leq 0.5$ppm, $H_2O \leq 0.5$ ppm) using a desiccant. **Figure 9** shows the dependence of the ESR spectrum of the HOD on the device operation with 365 nm-light irradiation at $J = 40$ mA cm^{-2} at RT. The data were obtained by averaging ESR spectra measured during the device operation for 1 h. In Figure 9a, the blue dotted and green solid lines show the ESR spectrum of the HOD before and after the device operation, respectively. Figure 9b shows the device-operation-induced ESR spectrum of the HOD after the device operation, which is obtained by subtracting the data before the device operation from that after the device operation. The obtained ESR parameters $g = 2.0040\pm0.0003$ and $\Delta H_{pp} = 1.16\pm0.02$ mT are consistent with those of the Signal B observed for the OLED. Thus, we have demonstrated that the same cationic decomposed Alq_3 molecules are observed in the HOD under UV exposure and that the interaction between NPB and Alq_3 can be eliminated. The high SN ratio of the ESR signal of the HOD indicates larger number of cationic decomposed Alq_3 molecules compared with those in the OLED, which is caused by large number of hole carriers in the HOD due to non-recombination with electron carriers.

2.6. Correlation between the Radical States and the Driving Voltage During Device Operation

Finally, we discuss the correlation between the radical states and the driving voltage of the same OLED by presenting the decrease in the Signal A during device operation. As mentioned above, although the formation of anionic Alq_3 has been reported to have no relation with the luminance decrease,[9] the intensity of the Signal A decreased slowly. However, the driving voltage of the OLED slowly increased as the duration of the device operation increased. To examine the correlation between the Signal A and the driving voltage, we compare the dependences of the N_{spin} of the Signal A and the driving voltage of the same OLED on the duration of the device operation. **Figure 10** shows the result, where the N_{spin} is plotted inversely for the vertical axis to clearly show the correlation. The driving voltage of the operating OLED increased gradually from 6.58 to 8.82 V, which demonstrates the correlation between the increase in the driving voltage and the decrease in the N_{spin} of the Signal A. As discussed above, the interface barriers are decreased due to the formation of anionic Alq_3 before the device operation. Thus, from this correlation, we suggest that the electron-injection barrier at the Alq_3/LiF/Al interfaces increased during device operation, because the use of LiF/Al for the cathode improves the efficiency of electron injection into Alq_3[28,29] and the Alq_3 radical anions are formed by the electron doping due to the reaction at the Alq_3/LiF/Al interfaces,[31,32] as mentioned above. In other words, the loss of anionic Alq_3 during device operation caused the increase in the driving voltage, which may be due to the oxidation of the anionic Alq_3 molecules during device operation.

3. Conclusions

We simultaneously measured the ESR signal and the luminance of the same OLED during device operation to elucidate the degradation mechanism in the operating OLEDs using the typical Alq_3-based OLED device of ITO/NPB/Alq_3/LiF/Al. The ESR spectrum changed by the device operation, which correlated with the luminance degradation. From the fitting analysis of the ESR spectrum and the DFT calculation, we found the evidence for the

formation of the radical anionic Alq_3 molecules before the device operation and the formation of the radical cationic decomposed Alq_3 molecules after the device operation. Thus, we strongly suggest that the luminance degradation in the OLEDs is due to the formation of the radical cationic decomposed Alq_3 molecules, not due to the radical formation of the decomposed NPB molecules. Also, the electron-injection barriers at the Alq_3/LiF/Al interfaces are found to increase from the correlation between the decrease in anionic Alq_3 and the increase in the driving voltage. The above elucidations of the radical states in OLEDs during device operation have been demonstrated at the molecular level for the first time. The correlation between the radical states and the performance degradation of the OLEDs at the molecular level would give deep insight into the mechanisms of the device operation and degradation, which would be effective for improving the device performance.

Received: ((will be filled in by the editorial staff))
Revised: ((will be filled in by the editorial staff))
Published online: ((will be filled in by the editorial staff))

[1] S. R. Forrest, *Nature* **2004**, *428*, 911.

[2] G. M. Farinola, R. Ragni, *Chem. Soc. Rev.* **2011**, *40*, 3467.

[3] M. Cai, T. Xiao, E. Hellerich, Y. Chen, R. Shinar, J. Shinar, *Adv. Mater.* **2011**, *23*, 3590.

[4] H. Uoyama, K. Goushi, K. Shizu, H. Nomura, C. Adachi, *Nature* **2012**, *492*, 234.

[5] H. Sasabe, J. Kido, *Eur. J. Org. Chem.* **2013**, *2013*, 7653.

[6] C. Sekine, Y. Tsubata, T. Yamada, M. Kitano, S. Doi, *Sci. Technol. Adv. Mater.* **2014**, *15*, 034203.

[7] C. W. Tang, S. A. VanSlyke, *Appl. Phys. Lett.* **1987**, *51*, 913.

[8] S. A. Van Slyke, C. H. Chen, C. W. Tang, *Appl. Phys. Lett.* **1996**, *69*, 2160.

[9] H. Aziz, Z. D. Popovic, N.-X. Hu, A.-M. Hor, G. Xu, *Science* **1999**, *283*, 1900.

[10] M. Nakahara, M. Minagawa, T. Oyamada, T. Tadokoro, H. Sasabe, C. Adachi, *Jpn. J. Appl. Phys. Lett.* **2007**, *46*, L636.

[11] H. Murata, A. S. D. Sandanayaka, *SID Symp. Digest Tech. Papers* **2014**, *45*, 32.

[12] D. Y. Kondakov, J. R. Sandifer, C. W. Tang, R. H. Young, *J. Appl. Phys.* **2003**, *93*, 1108.

[13] D. Y. Kondakov, *J. Appl. Phys.* **2008**, *104*, 084520.

[14] F. So, D. Kondakov, *Adv. Mater.* **2010**, 22, 3762.

[15] L. S. Liao, X. H. Sun, L. F. Cheng, N. B. Wong, C. S. Lee, S. T. Lee, *Chem. Phys. Lett.* **2001**, *333*, 212.

[16] T. Ikeda, H. Murata, Y. Kinoshita, J. Shike, Y. Ikeda, M. Kitano, *Chem. Phys. Lett.* **2006**, *426*, 111.

[17] K. Thangaraju, J. Kumar, P. Amaladass, A. K. Mohanakrishnan, V. Narayanan, *Appl. Phys. Lett.* **2006**, *89*, 082106.

[18] K. Thangaraju, P. Amaladass, K. Shanmuga Bharathi, A. K. Mohanakrishnan, V. Narayanan, J. Kumar, *Appl. Surf. Sci.* **2009**, *255*, 5760.

[19] F. P. Rosselli, W. G. Quirino, C. Legnani, V. L. Calil, K. C. Teixeira, A. A. Leitão, R. B. Capaz, M. Cremona, C. A. Achete, *Org. Electron.* **2009**, *10*, 1417.

[20] K. Marumoto, S. Kuroda, T. Takenobu, Y. Iwasa, *Phys. Rev. Lett.* **2006**, *97*, 256603.

[21] T. D. Pawlik, D. Y. Kondakov, W. J. Begley, R. H. Young, *J. SID* **2010**, *18*, 277.

[22] K. Marumoto, T. Fujimori, M. Ito, T. Mori, *Adv. Energy Mater.* **2012**, *2*, 591.

[23] D. Son, K. Marumoto, T. Kizuka, Y. Shimoi, *Synth. Met.* **2012**, *162*, 2451.

[24] D. Son, Y. Shimoi, T. Kizuka, K. Marumoto, *Jpn. J. Appl. Phys.* **2013**, *52*, 05DB07.

[25] T. Nagamori, K. Marumoto, *Adv. Mater.* **2013**, *25*, 2362.

[26] D. Son, Y. Shimoi, K. Marumoto, *Mol. Cryst. Liq. Cryst.* **2014**, *599*, 153.

[27] D. Son, T. Kuwabara, K. Takahashi, K. Marumoto, *Appl. Phys. Lett.* **2016**, *109*, 133301.

[28] B. N. Limketkai, M. A. Baldo, *Phys. Rev. B* **2005**, *71*, 085207.

[29] E. Ahlswede, J. Hanisch, M. Powalla, *Appl. Phys. Lett.* **2007**, *90*, 163504.

[30] T. Tsujimura, K. Furukawa, H. Li, H. Kashiwagi, M. Miyoshi, S. Mano, H. Araki, A. Ezaki, *SID Symp. Digest Tech. Papers* **2012**, *43*, 605.

[31] M. G. Mason, C. W. Tang, L.-S. Hung, P. Raychaudhuri, J. Madathil, D. J. Giesen, L. Yan, Q. T. Le, Y. Gao, S.-T. Lee, L. S. Liao, L. F. Cheng, W. R. Salaneck, D. A. dos Santos, J. L. Brédas, *J. Appl. Phys.* **2001**, *89*, 2756.

[32] C.-I Wu, G.-R. Lee, T.-W. Pi, *Appl. Phys. Lett.* **2005**, 87, 212108.

[33] K. Azuma, D. Son, K. Marumoto, M. Kijima, Y. Shimoi, *Chem. Lett.* **2012**, *41*, 191.

[34] Y. Tamai, H. Ohkita, M. Namatame, K. Marumoto, S. Shimomura, T. Yamanari, S. Ito, *Adv. Energy Mater.* **2016**, *6*, 1600171.
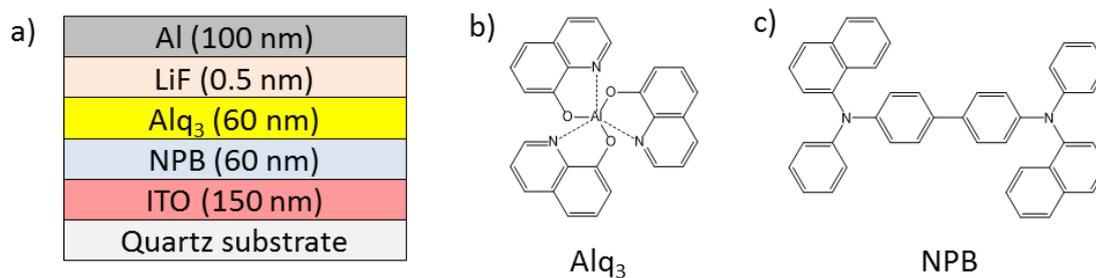
Figure 1. a) A schematic of the cross section of the OLED structure used in this study. Chemical structures of b) Alq$_3$ and c) NPB.
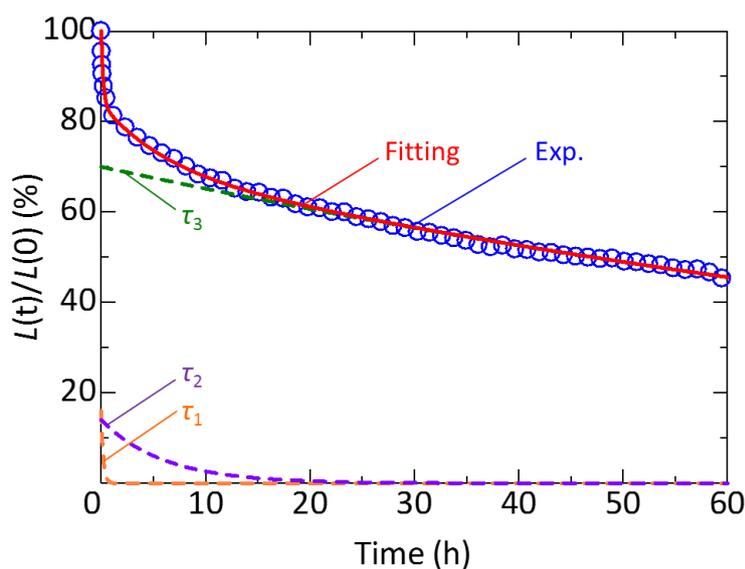

Figure 2. Dependence of the relative luminance (blue open circles) of the OLED on the duration of the device operation at a constant current density $J = 40$ mA cm^{-2} at room temperature (RT). Red solid line shows the fitting analysis obtained from the sum of three exponential functions: orange, purple, and green doted lines show each exponential function component.
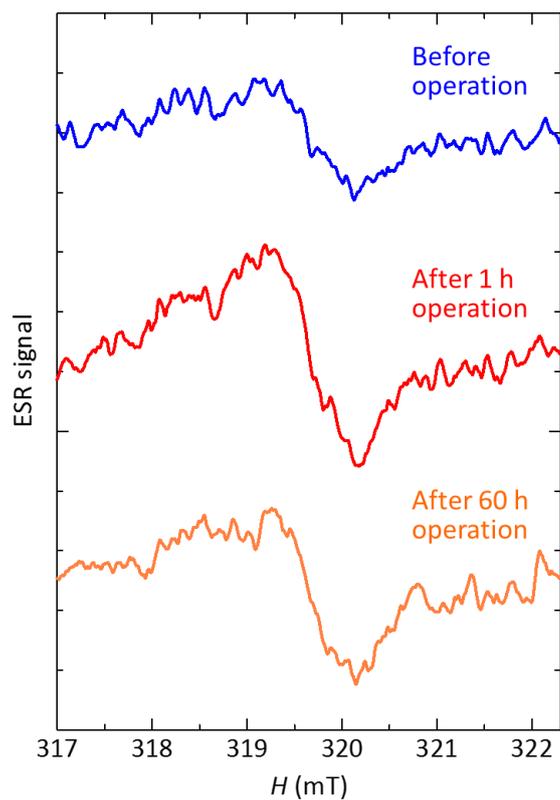
Figure 3. Dependence of the ESR spectrum of the OLED on the duration of the device operation at $J = 40$ mA cm^{-2} at RT. The upper data shows the spectrum before the device operation. The middle data shows the spectrum after 1 h device operation. The lower data shows the spectrum after 60 h device operation. The data were obtained by averaging ESR spectra measured during device operation for 1 h.
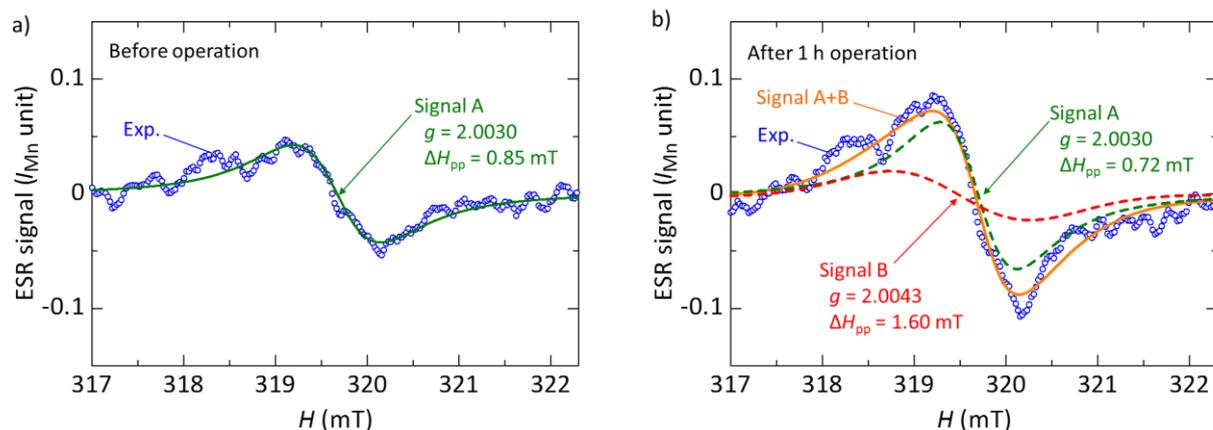
Figure 4. Fitting analyses of the ESR spectrum of the OLED before the device operation (a) and after 1 h device operation (b). The vertical axis is plotted using a unit of peak-to-peak ESR intensity of the ESR signal of a standard Mn^{2+} marker sample, I_{Mn}. a) The blue open circles show the experimental spectrum before the device operation. The green solid line shows the fitting result using a Lorentzian function. b) The blue open circles show the experimental spectrum after 1 h device operation. The green and red dotted lines show the fitting result using Lorentzian and Gaussian functions, respectively. The orange solid line shows the sum of these functions.
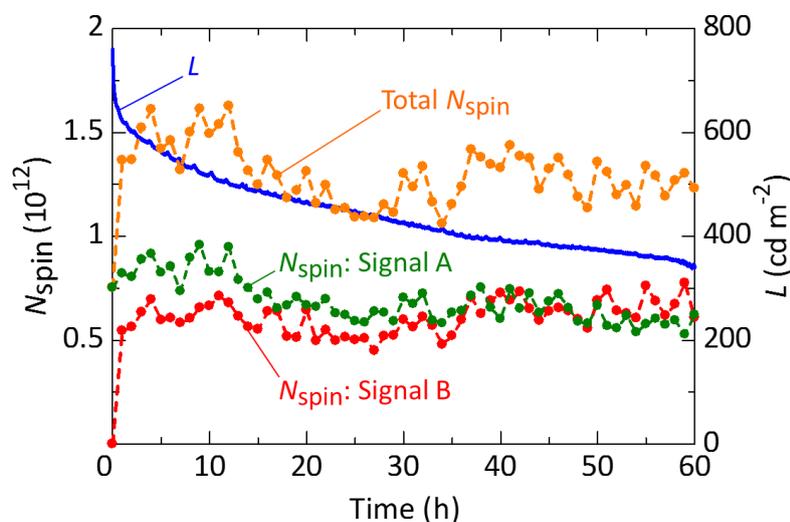

Figure 5. Dependence of the number of spins (N_{spin}) from the ESR signal and the luminance of the OLED on the duration of the device operation at $J = 40$ mA cm^{-2} at RT. The blue line shows the luminance. The green solid circles show the N_{spin} of the Signal A. The red solid circle show the N_{spin} of the Signal B. The orange solid circles show the sum of these components.
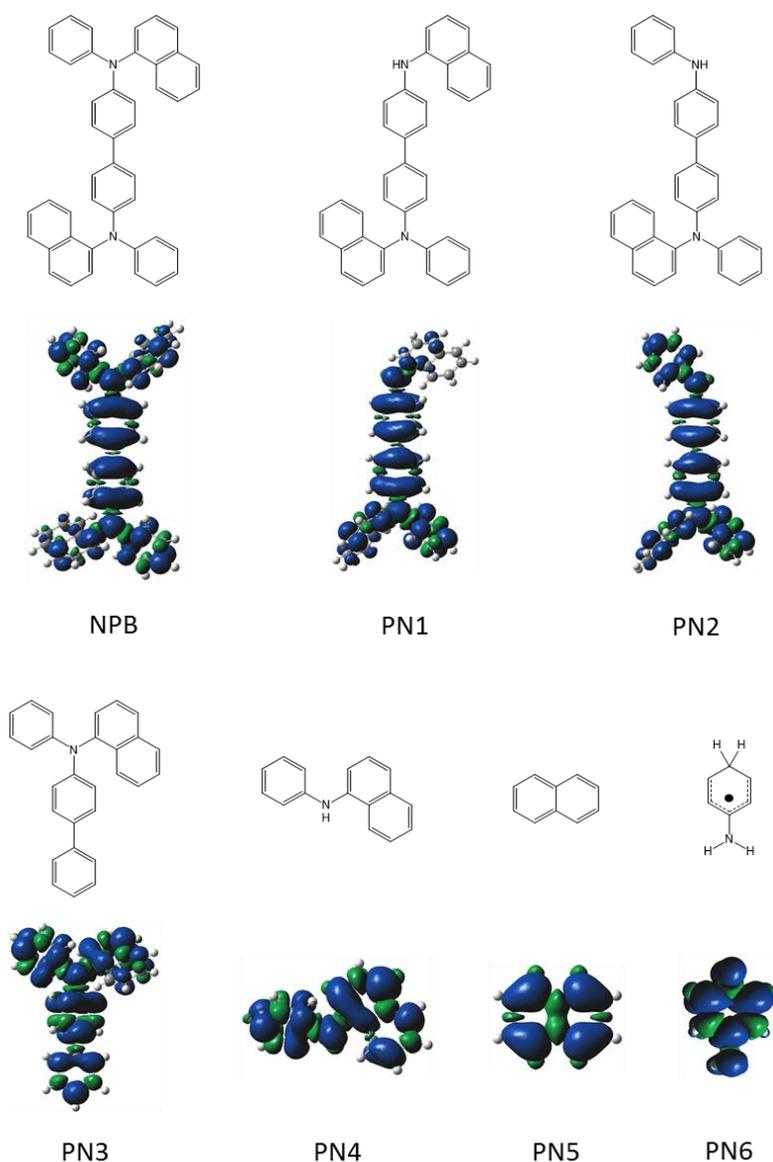
21

Figure 6. Chemical structures of NPB and tentative decomposed NPB molecules, and the spin density distribution obtained from the DFT calculation. For NPB and the decomposed NPB molecules PN1-PN5, the radical cationic states are calculated. For the decomposed NPB molecule PN6, the neutral radical state is calculated.
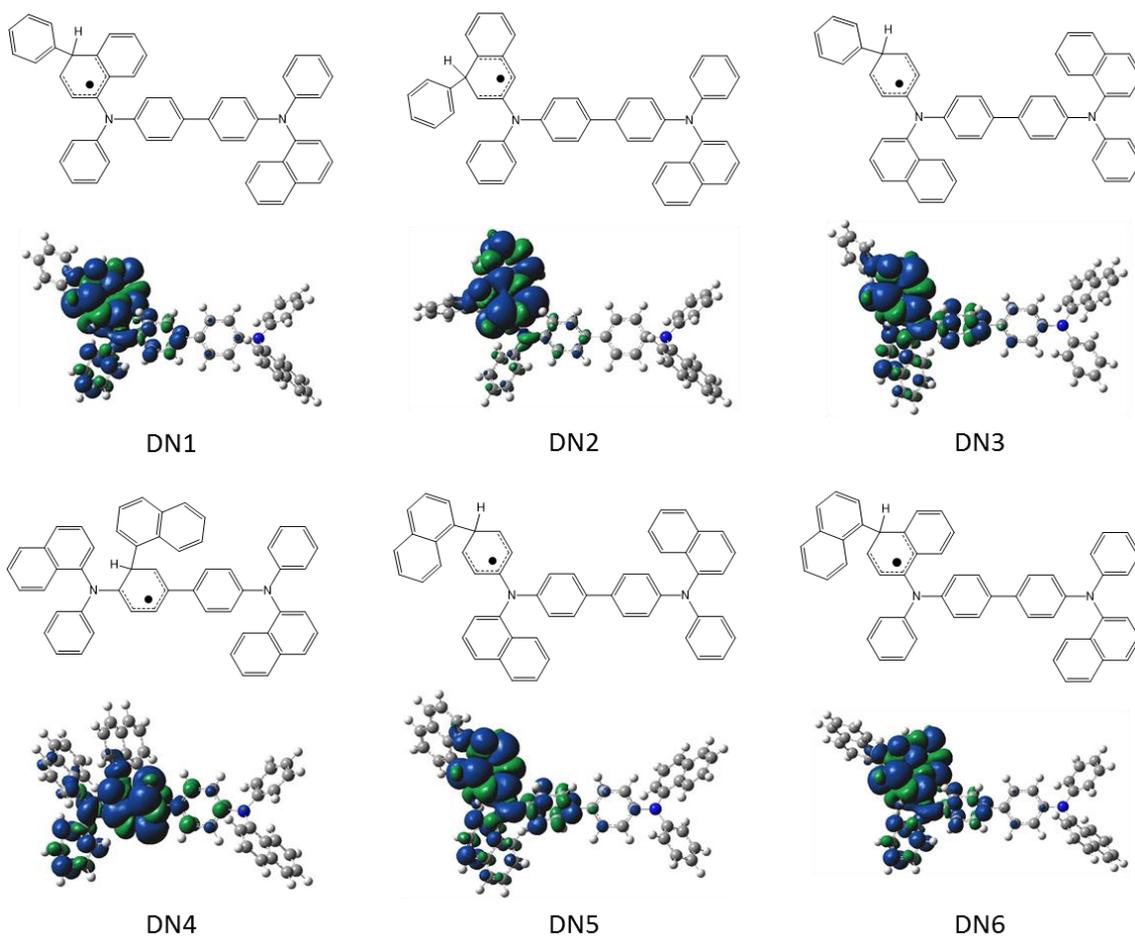
DN1

DN2

DN3

DN4

DN5

DN6

Figure 7. Chemical structures of tentative degraded NPB molecules, and the spin density distribution of these neutral radical states obtained from the DFT calculation.
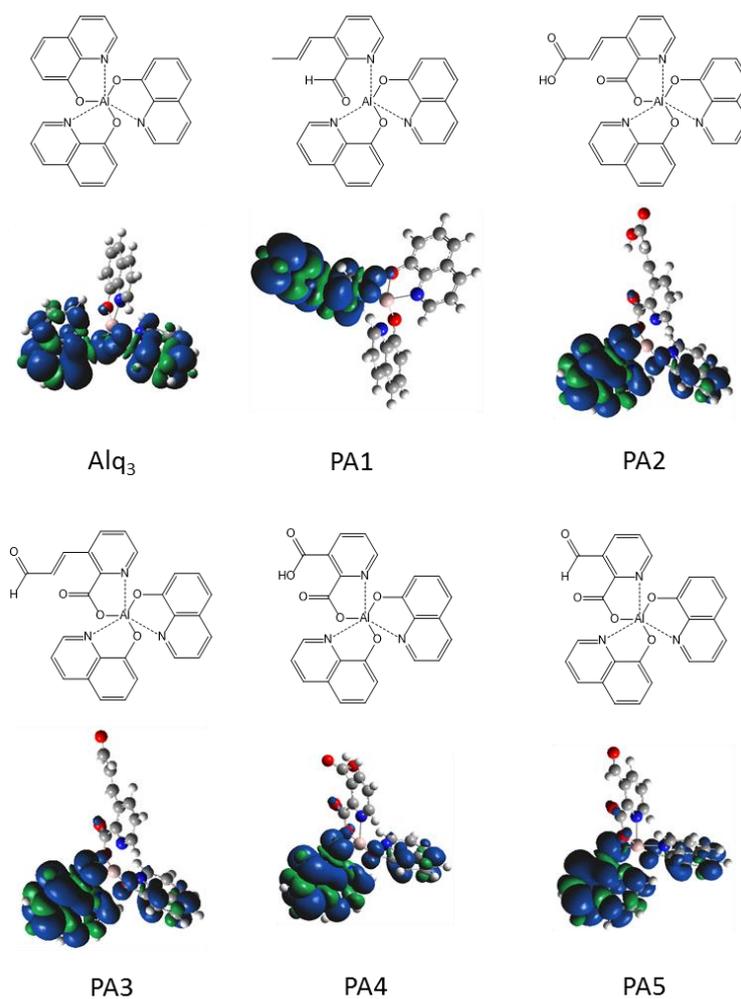
Figure 8. Chemical structures of Alq$_3$ and tentative decomposed Alq$_3$ molecules, and the spin density distribution of these radical cationic states obtained from the DFT calculation.
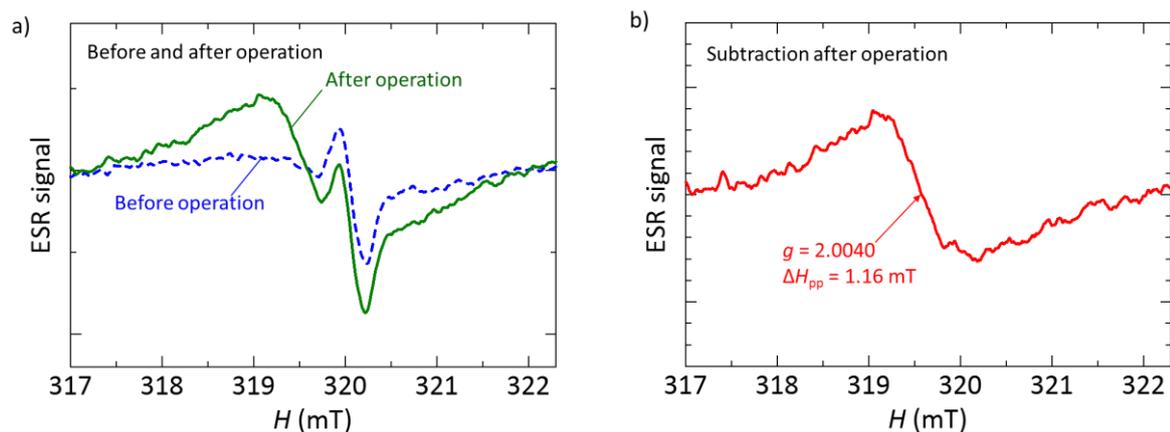
Figure 9. Dependence of the ESR spectrum of a hole-only device (HOD) of ITO/Alq₃/Au on the device operation with 365 nm-light irradiation at $J = 40$ mA cm^{-2} at RT. The data were obtained by averaging ESR spectra measured during the device operation for 1 h. a) The blue dotted and green solid lines show the ESR spectrum of the HOD before and after the device operation, respectively. b) Device-operation-induced ESR spectrum of the HOD after the device operation, which is obtained by subtracting the data before the device operation from that after the device operation.
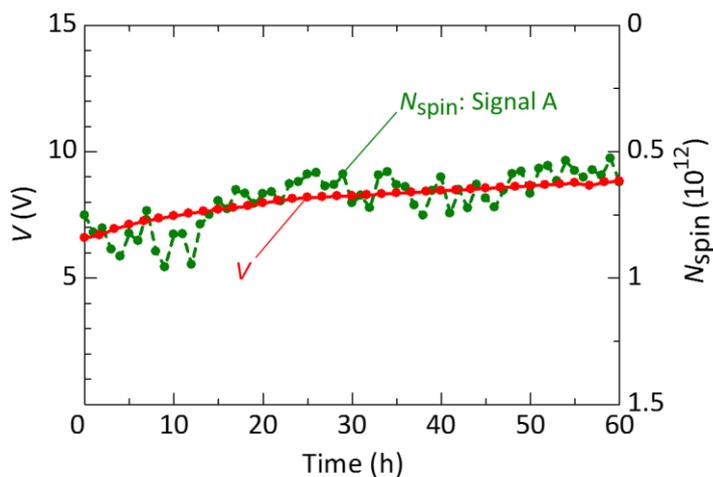

Figure 10. Dependence of the driving voltage (red solid circles) and the N_{spin} of the Signal A (green solid circles) of the OLED on the duration of the device operation at $J = 40$ mA cm^{-2} at RT. The N_{spin} is plotted for the inverse vertical axis.

25

Table 1. Calculated principal values of the g tensor (g_1, g_2, g_3) for NPB and tentative decomposed NPB molecules from the DFT calculation. For the NPB and the decomposed NPB molecules PN1-PN5, a radical cationic state is calculated. For the decomposed NPB molecule PN6, a neutral radical state is calculated. An average of the principal values g_{avg} was calculated as $g_{ave} = \sqrt{g_x^2 \langle l^2 \rangle + g_y^2 \langle m^2 \rangle + g_z^2 \langle n^2 \rangle}$ using $l = \sin\theta\cos\phi$, $m = \sin\theta\sin\phi$, and $n = \cos\theta$, where $< >$ represents spatial average. Here random orientation of molecules was assumed to calculate the g_{ave}.

Calculated molecule	g_1	g_2	g_3	g_{ave}
NPB	2.0025	2.0028	2.0034	2.0029
PN1	2.0023	2.0027	2.0035	2.0028
PN2	2.0025	2.0028	2.0034	2.0029
PN3	2.0024	2.0029	2.0032	2.0028
PN4	2.0024	2.0028	2.0033	2.0028
PN5	2.0024	2.0026	2.0030	2.0027
PN6	2.0021	2.0029	2.0032	2.0027

Table 2. Calculated principal values of the g tensor (g_1, g_2, g_3) and the g_{ave} for the neutral radical states of tentative degraded NPB molecules DN1-DN6 from the DFT calculation.

Calculated molecule	g_1	g_2	g_3	g_{ave}
DN1	2.0022	2.0028	2.0029	2.0026
DN2	2.0021	2.0028	2.0029	2.0026
DN3	2.0022	2.0029	2.0029	2.0027
DN4	2.0022	2.0028	2.0030	2.0027
DN5	2.0022	2.0029	2.0030	2.0027
DN6	2.0022	2.0028	2.0030	2.0026

Table 3. Calculated principal values of the g tensor (g_1, g_2, g_3) and the g_{ave} for the radical cationic states of Alq_3 and the decomposed Alq_3 molecules PA1-PA5 from the DFT calculation.

Calculated molecule	g_1	g_2	g_3	g_{ave}
Alq_3	2.0029	2.0038	2.0055	2.0041
PA1	2.0022	2.0032	2.0034	2.0029
PA2	2.0028	2.0041	2.0052	2.0040
PA3	2.0027	2.0041	2.0052	2.0040
PA4	2.0027	2.0041	2.0052	2.0040
PA5	2.0028	2.0040	2.0052	2.0040